

# Constraints on source and lens parameters from microlensing variability in QSO 0957+561 A,B

S. Refsdal<sup>1,5</sup>, R. Stabell<sup>2,5</sup>, J. Pelt<sup>3,5</sup>, and R. Schild<sup>4,5</sup>

<sup>1</sup> Hamburger Sternwarte, Gojenbergsweg 112, D-21029 Hamburg, Germany

<sup>2</sup> Institute of Theoretical Astrophysics, University of Oslo, P.O. Box 1029, Blindern, N-0315 Oslo, Norway

<sup>3</sup> Tartu Observatory, 61602 Toravere, Estonia

<sup>4</sup> Harvard-Smithsonian Center for Astrophysics, MS-19 60 Garden Street Cambridge, MA 02138, USA

<sup>5</sup> Centre for Advanced Study, Drammensveien 78, N-0271, Oslo, Norway

Received 28.02.2000, accepted ....

**Abstract.** From regular monitoring of the Double Quasar QSO 0957+561 A,B there is now general agreement on a time delay of about 416 days. This has made it possible to determine the microlensing residual in the light-curve, see Pelt et al. (1998). We have used two significant microlensing features: 1) A “quiet” period with a variability less than 0.05 mag lasting about 8 years, and 2) A change in the residual of 0.25 mag during a time interval of about 5 years. The first feature gives a lower limit for the lens mass,  $M$ , for a given normalized source radius,  $r$ , whereas the second feature gives an upper limit. We have considered the amount of mass in a continuum to be a free parameter with possible values between 0% (all mass in lenses) and 90%. At a significance level of 1% the mass can only be constrained within a rather wide range ( $10^{-6}M_{\odot}$  to  $5M_{\odot}$ ). For the radius  $R$  of the source an upper limit of  $10^{16}$  cm is found, whereas the normalized source radius  $r$  is restricted to be smaller than 30. At a level of 10% , however, the range of possible masses is much narrower ( $2 \cdot 10^{-3}M_{\odot}$  to  $0.5M_{\odot}$ ), and the upper limit of  $R$  is about  $6 \cdot 10^{15}$  cm, whereas the value of  $r$  is restricted to be less than 2. We have used an effective transverse velocity  $V$  equal to  $600 \text{ km s}^{-1}$ .

**Key words:** gravitational lensing – quasars: individual: QSO 0957+561

## 1. Introduction

The double quasar Q0957+561 A,B was the first discovered multiple image gravitational lens, the first to have a measured time delay and to produce a gravitational lens determination of the Hubble parameter, and the first system in which a microlensing effect was seen in the observational brightness record (Vanderriest et al. 1989). This was not unexpected since such microlensing effects had already been predicted by Chang & Refsdal (1979), see

also Kayser et al. (1986), hereafter referred to as KRS, and Schneider & Weiss (1987). With the time delay confirmed by the Vanderriest et al. report, Schild & Smith (1991) noted evidence for fine structure in the microlensing light-curve. In this paper we do not concern ourselves with this reported fine structure, and focus instead on the long-term microlensing trends.

After a period of controversy about the correct time delay value, Kundić et al. (1996) observed an unusually distinct event in the light curve of image A which repeated in image B 417 days later. This time delay was very close to the values obtained earlier by Vanderriest et al. (1989), Schild & Smith (1991) and Pelt et al. (1996), and has later been confirmed with high precision by other workers, see for instance Pelt et al. (1998) who found a time delay of 416.3 days. A precise value of the time delay is necessary in order to subtract out the intrinsic quasar brightness fluctuations on all time scales, and to find the microlensing residual.

The most accurate determination of microlensing variability in Q0957+561 was reported by Pelt et al. (1998). This variability is shown in Fig. 1 (their Fig. 9). Two principal features are seen in the 15 year microlensing light-curve: a rise of 0.25 mag during a period of about 5 years (1982-1986) with a maximum slope of 0.07 mag per year, and a quiet phase of about 8 years (1988-1996) with a variability less than 0.05 mag. The original data in Pelt et al. (1998) show a large scatter which has sometimes been suggested to evidence microlensing on time scales of 100 days and shorter (Schild 1996) but the existence of such low amplitude and rapid fluctuations is complicated by questions of the accuracy of the data; we therefore restrict our analysis to the less controversial long-term microlensing. Although gaps as long as 300 days are present in the long-term microlensing record, segments where the brightness record is more intensively sampled seem to show that amplitudes on sub-year timescales are less than 5% and they average away as shown convincingly in the Pelt et al. (1998) Fig. 9 plot.

This paper is concerned with understanding the two features in the light-curve mentioned above, from models of the gravitational lens and microlensing from stars or other compact objects presumed to lie within the lens galaxy G1. For typical quasar accretion disc sizes it is possible that statistical effects from numerous stars projected in front of the quasar must be considered; a statistical microlensing theory for such a case can be found in Refsdal & Stabell (1991 (RS1), 1993 (RS2) and 1997).

From macro-lens modeling of Q0957+561 one finds the lensing optical depth for the A and B image to be  $\kappa_A = 0.22$  and  $\kappa_B = 1.24$ , respectively, and with shear terms  $\gamma_A = \pm 0.17$  and  $\gamma_B = \pm 0.9$  (Lehar, private communication; see also Schmidt & Wambsganss (1998) for similar estimates and a definition of the shear). Our source model is circular with a Gaussian distributed surface luminosity and “radius”  $R$ .

We shall treat three different mass models in our microlensing simulations:

Case 1: All the lensing mass is in identical compact microlenses with mass  $M$ .

Case 2: 10% of the lensing mass is in identical compact lenses with mass  $M$  and 90% in an evenly distributed continuum.

Case 3: 10% of the lensing mass is in compact lenses with  $1 M_\odot$  and 90% in compact lenses with mass  $M < M_\odot$ .

Our approach is to compare simulated microlensing light-curves with the observed microlensing variability. Because the lens mass  $M$  and the source radius  $R$  both affect the amplitude and time scale of variability, we find some interesting constraints for these two parameters in the lens system Q0957+561.

Schmidt & Wambsganss (1998) have examined the available parameter space based upon an observed quiet period of 160 days with a variability less than 0.05 mag.

The results of our study are based on the microlensing variability during 15 years, including a long quiet phase as well as a significant event and naturally gives stronger constraints.

## 2. Observed microlensing variability

We make use of the observed microlensing light-curve covering a time span  $T = 15$  years, see Fig.1. The curve is given by:

$$m(t) = m_A - m_B^\tau \quad (1)$$

where  $m_B^\tau$  is the magnitude of the B image shifted by the time delay  $\tau = 416.3$  days (see Pelt et al. 1998). Two significant microlensing features are found:

1) A “quiet” period with a variability  $\delta m = m_{\max} - m_{\min}$  less than 0.05 mag lasting  $\delta t = 8$  years.

2) A variation of  $\Delta m = 0.25$  mag during a time interval  $\Delta t = 5$  years, with a maximum slope of about 0.07 mag/year (“the event”).

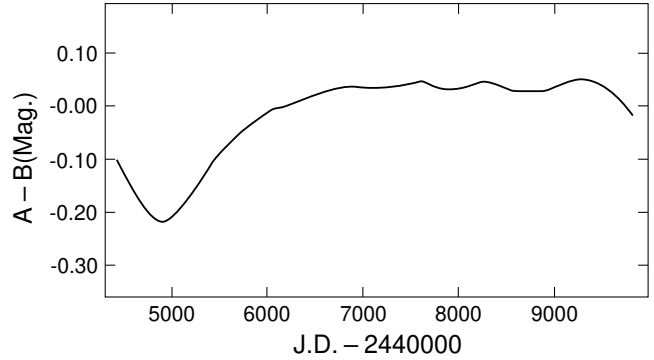


**Fig. 1.** Observed microlensing light-curve for QSO 0957+561,  $m(A)$  minus the timeshifted  $m(B)$ , showing an event of 0.25 mag lasting 5 years and a quiet phase with a variability  $\delta m$  less than 0.05 lasting 8 years

We shall treat these two features independently and investigate by means of simulations how lens and source parameters can be constrained. The results will be demonstrated in “exclusion diagrams”, see Figs. 2 and 3.

Since the optical depth is much larger for the B image than for A, the microlensing variability in the A image is likely to be much smaller than in the B image. We shall therefore in this paper neglect a possible microlensing variability in the A image and assume that the observed microlensing variability comes only from B. From test calculations we find that this approximation has a rather small influence on the constraints obtained (see Discussion).

## 3. Case 1: all mass in identical lenses

We shall first choose all mass to be in lenses with mass  $M$ . This may not be very realistic, but it allows a relatively simple discussion with only two free parameters ( $M$  and source radius  $R$ ), and it gives us an understanding which is quite useful also for more complex mass distributions. We simulated light-curves for the B image with effective transverse motion of the source parallel to the shear and perpendicular to the shear ( $\gamma_B = \pm 0.9$ ). The results for these two cases are always sufficiently similar so that an intermediate case easily can be interpolated. For practical reasons we shall instead of  $R$  use the normalized source radius  $r = R/R_E$  as a free parameter, where  $R_E$  is the Einstein radius (for mass  $M$ ), projected into the source plane

$$R_E = \sqrt{\frac{4GM}{c^2} \frac{D_{ds} D_s}{D_d}} = 4.8 \cdot 10^{16} \sqrt{\frac{M}{M_\odot h_{60}}} \text{ cm} \quad (2)$$

Here the  $D$ 's are angular size distances and  $h_{60}$  is the dimension-less Hubble parameter,  $h_{60} = H_0 / (60 \text{ km s}^{-1} \text{ Mpc}^{-1})$ . We have used a cosmological model with  $\Omega = 0.5$  and  $\Lambda = 0$ .

For randomly distributed compact lenses we simulate light-curves for different values of the normalized source

radius  $r$ , using well known ray tracing techniques, see KRS and Schneider & Weiss (1987). We obtain for each value chosen for  $r$  the magnitude of the source as a function of the normalized source position:  $m = m(y)$ , where  $y = \eta/R_E$  and  $\eta$  is the length coordinate along the source track. For each value of  $r$  we get the light-curve for different (but still all identical)  $M$ -values by a transformation of  $y$  to the time  $t$  measured by the observer. For our system we find

$$t = 25y v_{600}^{-1} \sqrt{\frac{M}{M_\odot h_{60}}} \text{ years} \quad (3)$$

Here  $v_{600} = V/(600 \text{ km s}^{-1})$  where  $V$  is the effective transverse velocity of the source assumed to be constant, with time measured by the observer, see KRS. When not stated otherwise we shall use  $v_{600} = 1$  and  $h_{60} = 1$  in this paper.

Since  $t \propto y \sqrt{M}$  the light-curves are simply stretched out in time for larger values of  $M$ . Hence, it is not necessary to calculate light-curves for different  $M$ -values (for a given  $r$ ). We have therefore simulated light-curves only for various  $r$ -values ( $r=0.02, 0.05, 0.1, 0.3, 1, 3, 5, 10, 20$  and  $50$ ). The length of the light-curves corresponds in most cases to at least 1000 years for the allowed masses, see Eqs. (3) and (4). We first discuss the constraints on  $M$  and  $R$  (and  $r$ ) which can be obtained from the quiet phase of 8 years.

#### i) Quiet phase constraints

For each value of the normalized source radius  $r$  we calculate the microlensing light-curve  $m(y)$  for  $\kappa = \kappa_B = 1.24$  and  $\gamma = \gamma_B = \pm 0.9$ . Giving equal weight to the two shear directions we can then determine the probability  $P_q(M, r)$  to obtain a quiet period lasting at least 8 years during a period of 15 years with a variability  $\delta m = m_{\max} - m_{\min}$  less than 0.05 mag. Since  $t$  is proportional to  $y \cdot \sqrt{M}$ , the probability  $P_q(M, r)$  obviously increases monotonically with  $M$ . Hence, we can determine a critical mass  $M_q(r)$  by requiring that  $P_q(M_q, r)$  is, say 0.01. We then choose to exclude values of  $M(r)$  less than  $M_q(r, P_q)$  since the probability of getting a quiet period of 8 years or more is then less than one percent (compare the paper by Schmidt & Wambsganss, 1998). The dependence of  $M_q$  on  $r$  for  $P_q = 0.01$  is shown in the exclusion diagram in Fig. 2 as the solid line to the left labeled **q**.

We can roughly distinguish 3 different parts of the curve  $M_q(r, 0.01)$ :

1)  $r < 0.5$  : Here we find  $M_q$  very nearly constant and equal to about  $0.05 M_\odot$ . This corresponds to  $R_E \approx 10^{16}$  cm and  $\tau_E = R_E/V \approx 5$  years.

The behavior with an almost constant  $M_q$  (and  $R_E$  and  $\tau_E$ ) for small values of  $r$  is a consequence of the nearly identical light-curves for different (small)  $r$  with the same star field. Only during caustic crossings will there be a major difference in the light-curves, but then the variability will be large anyway and therefore violate the quiet phase condition. For small  $r$  the probability of getting a

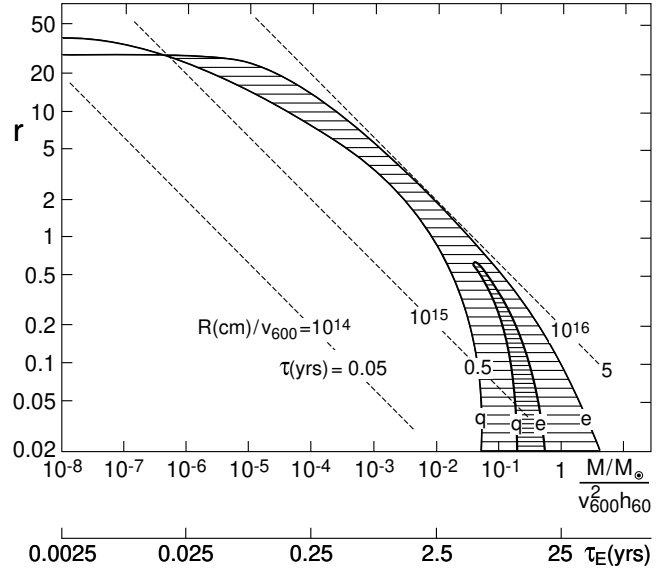


**Fig. 2.** Exclusion diagram for the case when all mass is in lenses of identical masses (Case 1). The constraint curves for the quiet phase (**q**) and the event (**e**) are shown in the  $(M, r)$ -plane. The allowed region for significance level 0.01 is hatched and for significance level 0.1 more densely hatched. Note that the mass values scale with the effective transverse velocity and the Hubble parameter.

quiet phase therefore only depends on  $M$  so that  $M_q$  is nearly independent of  $r$  for  $r < 0.5$ .

2)  $0.5 < r < 10$  : Here we find that  $M_q$  is roughly proportional to  $r^{-2}$ . Since  $r = R/R_E \propto R/\sqrt{M}$  this means that  $R$  is roughly constant in this range. We find here  $R \approx 4 \cdot 10^{15}$  cm and  $\tau = R/V \approx 2$  years. This result is not unexpected, since the variability time scale for sources with  $r > 1$  is about equal to  $2\tau$ , see RS2.

3) For  $r > 10$  the curve gets flatter and approaches asymptotically a maximum value of  $r_{qm} \approx 40$ . Such an asymptotic behavior was to be expected from the results in RS1, where it was shown that microlensing amplitudes for large sources ( $r \gg 1$ ) are proportional to  $r^{-1}$ .

#### ii) Event constraints

In the simulated light-curves we consider only events with a variability between 0.2 mag and 0.3 mag ( $\Delta m \pm 0.05$ ), and with a maximum slope during the event steeper than 0.07 mag per year. The reason for choosing also an upper limit for the allowed event magnitudes is that the simulated events for small values of  $r$  typically show larger amplitudes than the observed one. In our analysis we have found it more practical to use the maximum slope rather than the time scale  $\Delta t$ . We can then estimate the probability  $P_e(M, r)$  of getting such an event during a time span of  $T = 15$  years. Since the slope scales as  $M^{-0.5}$  and the simulated time span as  $M^{0.5}$ , it is clear that  $P_e(M, r)$  decreases monotonically with increasing  $M$ . We can therefore determine a critical mass  $M_e(r)$  by requiring that

$P_e(M_e, r)$  is, say 0.01. We then choose to exclude values of  $M(r)$  larger than  $M_e(r, P_e)$ .

The dependence of  $M_e$  on  $r$  for  $P_e = 0.01$  is shown in Fig. 2 as the solid line to the right labeled **e**. It is seen that  $M_e(r)$  is roughly proportional to  $r^{-2}$ , and therefore  $R$  is fairly constant over a large range of  $r$ -values ( $0.2 < r < 10$ ). We get here  $R \approx 10^{16}$  cm and  $\tau = R/V = 5$  years. This is easy to understand since a typical event time scale is the crossing time  $2R/V$  for large sources (see RS2) as well as for small sources (caustic crossings).

For small  $r$ -values we see that the  $M_e$ -curve departs from  $R \approx$  constant towards smaller values of  $R$ , approaching a constant  $M_e$ -value of about  $5M_\odot$  for very small  $r$ . The reason is that for such small  $r$ -values, caustic crossing events as small as  $\Delta m \approx 0.25$  are quite rare. Of some importance here are, however, some non-caustic events, typically occurring when the track passes just outside a cusp of a caustic. For very small sources ( $r < 0.1$ ) these events are nearly independent of  $r$ , which can explain that  $M_e(r)$  stays nearly constant for these small  $r$ -values. We note that the time scale for these events are usually longer than the crossing time  $2R/V$ , see also Wyithe et al. (1999).

For very small  $r$ -values the effect of the so-called ghost caustics which are produced when two lens masses are very close to each other is also of importance, (Grieger et al. 1989, Wambsganss & Kundić 1995). These weak caustics can often “produce” events during caustic crossings as small as about 0.25 mag, even for very small  $r$ -values. An uncertainty arises, however, because relative motion of the stars some times causes large velocities of the ghost caustics so that the “ghost events” will occur more often and on a shorter time scale. Since we have not considered relative motion in our calculations, we may have underestimated the frequency and overestimated the time scale of ghost events. In that case the upper limit for  $M_e$  has been underestimated.

For large  $r$ -values the  $M_e$ -curve also departs from  $R \approx$  constant towards smaller values of  $R$  and approaches asymptotically a maximum  $r$ -value of about  $r_{em} = 30$ . This high value of  $r_{em}$  were to be expected from the results in RS2, where it was shown that quite significant events can be produced for rather large values of  $r$ .

iii) The allowed region

From the discussion in section i) we found that the quiet phase constraint gives a lower limit,  $M_q(r)$  for the lens mass. In section ii) on the other hand, the event constraint gave an upper limit  $M_e(r)$ . Hence, at a significance level of  $P$  we are left with an allowed region between the  $M_e$  and  $M_q$ -curves in the  $(M, r)$ -plane which fulfills

$$M_q(r, P) < M(r) < M_e(r, P) \quad (4)$$

For  $P = 0.01$  the allowed region is shown hatched in Fig. 2. For  $r$  between 0.5 and 20 we find a strip within a relatively narrow range of  $R$ -values ( $4 \cdot 10^{15}$  cm  $< R < 10^{16}$  cm), covering  $M$ -values between  $10^{-6}M_\odot$  and  $10^{-1}M_\odot$ .

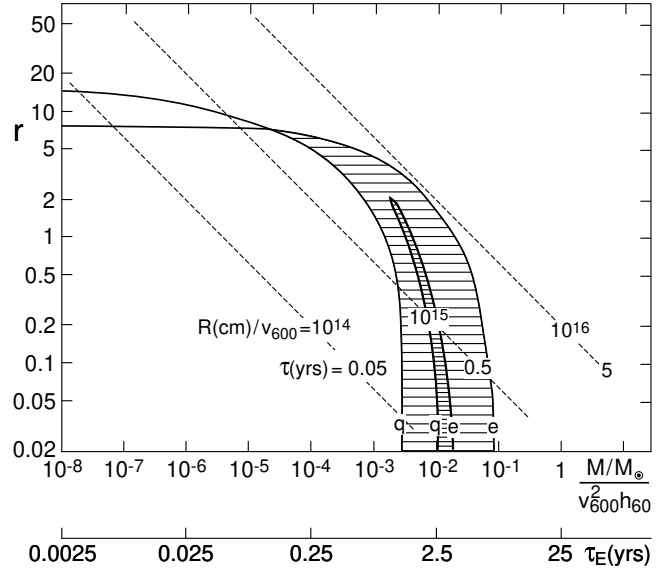


**Fig. 3.** Same as Fig. 2, but with 90% of the lens mass in a continuum (Case 2)

For  $r < 0.5$ , mass values between  $3 \cdot 10^{-2}M_\odot$  and  $1M_\odot$  are usually allowed. For the smallest  $r$ -values the upper limit reaches about  $5M_\odot$ . We cannot give a reliable lower limit of  $r$ . However, the lack of any clear high magnification events in all observed quasar light-curves is an argument against too small  $r$ -values (and  $R$ -values) for QSOs in general.

For larger  $P$ -values the allowed region obviously decreases. As an example the allowed region for  $P = 0.1$  is shown more densely hatched in Fig. 2. It is interesting to note that Eq. (4) can now only be fulfilled for  $r < 0.6$  and the possible mass shrinks approximately to the interval between  $0.05 M_\odot$  and  $0.5 M_\odot$  (significance level of 10%, and all mass in identical lenses).

#### 4. Case 2: 90% of the lensing mass in a continuum

Since a large fraction of the lens mass may be in a smoothly distributed continuum, we have repeated most of the calculations in the previous section, but now with 90% of the mass in a continuum and the remaining 10% in compact lenses with mass  $M$ . The resulting constraint curves are shown as solid lines in Fig. 3 for a significance level of 0.01, and the allowed region is hatched. We find that the asymptotic maximum  $r$ -values  $r_{qm}$  and  $r_{em}$  decrease with a factor of about 3 relative to Case 1. This was to be expected because the variability amplitude for large  $r$  is proportional to  $\sqrt{\kappa_s}/r$ , so that  $r_{qm}$  and  $r_{em}$  should be proportional to  $\sqrt{\kappa_s}$ , see RS1. Here  $\kappa_s$  is the optical depth for microlensing which is now a factor of 10 smaller than in Case 1.

The possible mass range is now restricted to an interval between  $3 \cdot 10^{-5}M_\odot$  and  $10^{-1}M_\odot$ .

For  $P = 0.1$  the allowed region is shown more densely hatched. We see that the possible mass now only covers an interval between  $2 \cdot 10^{-3} M_{\odot}$  and  $2 \cdot 10^{-2} M_{\odot}$ , and  $r$  is restricted to be less than about 2.

### 5. Case 3: Two lens populations

From the observed light and spectrum of the lensing galaxy we know that some of the mass must be in stars with typically one solar mass. We have therefore investigated a model with two lens populations; 10% of the mass in solar mass stars and the rest of the mass in objects of smaller mass,  $M$ . Treating as before  $M$  and  $r = R/R_E(M)$  as free parameters we get mostly small changes (relative to Case 1) in the constraint curves in the  $(M, r)$ -plane. The  $M_q$ -curves are almost unchanged, since the few  $1M_{\odot}$  stars can only make a minor change in the probability of getting long quiet phases for  $M < 1M_{\odot}$ . The  $M_e$ -curves also follow very closely the corresponding curves for Case 1 (with all mass in identical stars). A separate discussion of this case is therefore not necessary.

### 6. Change of $V$ and $H_0$

We have until now assumed specific values of the effective transverse velocity  $V$  and the Hubble parameter  $H_0$  ( $v_{600} = 1$  and  $h_{60} = 1$ ). It is easy to see what happens if these values are changed. If for example the transverse velocity is increased by a factor  $F$ , an identical light-curve is obtained if the source size  $R$  and the Einstein radius  $R_E$  are increased by the same factor, such that  $r = R/R_E$  is unchanged. Increasing the Einstein radius by a factor  $F$  means that each lens mass is increased by a factor  $F^2$ , and to keep the optical depth for lensing unchanged, the linear size of the lens field must of course be scaled up with a factor  $F$ .

Correspondingly, an increase of the Hubble parameter with a factor  $F$  can be compensated by an increase of each lens mass with the same factor to keep the light-curve unchanged. Since the Einstein radius is unchanged in this case, the optical depth is also unchanged, and no change in the size of the lens field is necessary.

According to the above discussion, the allowed regions in Figs. 2 and 3 will be shifted in mass when  $V$  and  $H_0$  are changed.

$$M_q(r) \propto V^2 H_0 \quad (5)$$

$$M_e(r) \propto V^2 H_0 \quad (6)$$

This is most conveniently taken into account by just scaling the mass coordinate appropriately, thereby leaving the curves in Figs. 2 and 3 in the same positions. Obviously the dominating uncertainty in  $M$  comes from the  $V^2$  term.

### 7. Discussion

By means of the two features in the microlensing light-curve for the Q0957+561 system and numerical simulations, we have shown that it is possible to set constraints on some parameters for the lens system. With the amount of the continuum mass between 0% (Case 1) and 90% (Case 2) we find the possible lens masses to have values between  $10^{-6} M_{\odot}$  and  $5M_{\odot}$  (1% level) and between  $2 \cdot 10^{-3} M_{\odot}$  and  $0.5M_{\odot}$  (10% level). The maximum source radius is found to be  $10^{16}$  cm (1% level) and  $6 \cdot 10^{15}$  cm (10% level). By including Case 3 (giving approximately the same results as Case 1), we find only negligible changes in the above limits.

From the two features in the microlensing light-curve it seems not possible to give a lower limit of  $R$ . The reason for this is that the light-curves for very small (but different) values of  $r$  are very similar, except during caustic crossings, and then the quiet phase constraint is violated anyhow.

From lens arguments based on the Q0957+561 light-curve alone, we can therefore not rule out very small  $r$ -values (even those much smaller than 0.02), and hence very small  $R$ -values. However, the lack of any clear high magnification events in observed quasar light-curves is an argument against too small  $r$ -values (and  $R$ -values) for QSOs in general.

We have in this paper only considered microlensing effects in the B image. The combined A and B microlensing light-curve will statistically show slightly more variability and less chance of extended quiet phases, and have a slightly higher rate of events than for B alone. Hence, both  $M_q$  and  $M_e$  will increase slightly. Our test calculations indicate a rather small effect of about 10%.

Since we have neglected the relative motion of the lens masses we may have underestimated the maximum allowed lens mass which occur for small values of  $r$ , particularly in Case 1. This ought to be investigated in the future.

We have in this investigation considered the two features found in the light-curve for Q0957+561 independently and used the probabilities  $P_q$  and  $P_e$  separately. An alternative approach, which would have given much stronger constraints, might have been to consider the probability for both features to be found within a period of 15 years which must be less than  $P_q \cdot P_e$ . The largest values of  $P_q \cdot P_e$  (between 0.01 and  $\approx 0.02$ ) are obviously found within the densely hatched regions in Fig. 2 (Case 1) and Fig. 3 (Case 2). The most probable mass values would then mainly depend on the amount of mass in the continuum ( $\approx 0.3M_{\odot}$  in Case 1 and  $\approx 0.01M_{\odot}$  in Case 2), and the most probable  $r$ -value is less than 1. It is, however, not possible to give levels of significance here since we are obviously doing a posteriori statistics. It seems in fact difficult to avoid a posteriori statistics when making use of a larger part of the information in the light-curve.

Wyithe et al. (1999) have published a series of papers (see astro-ph/9911245 and references therein) where they make use of the distribution of the microlensed light-curve derivatives, and they apply the method on the QSO 2237+0305 light-curve. Their method does not suffer from a posteriori statistics, but more information in the light-curve could perhaps have been taken into account, for instance the correlation time-scale for the derivatives, without running this risk. A comparison with their results is, however, difficult since they are considering a different system. For their system the value of  $R_E$  is about a factor of 3 larger, whereas the source radius  $R$  is roughly a factor 2.5 smaller (estimated from the difference in intrinsic luminosity). Hence, the normalized source radius  $r = R/R_E$  will be a factor of about 7 smaller. With this factor in mind we do not see any serious conflict between the rather small  $R$ -values they obtain and our (most probable) values.

## References

- Chang K., Refsdal S., 1979, Nat 282, 561  
Grieger B., Kayser R., Refsdal S., Stabell R., 1989, Abhandlungen aus der Hamburger Sternwarte, Band X, Heft 4  
Kayser R., Refsdal S., Stabell R., 1986, A&A 166, 36 (KRS)  
Kundić T., Turner E.L., Colley W.N., et al., 1996, ApJ 482, 75  
Pelt J., Kayser R., Refsdal S., Schramm T., 1996, A&A 305, 97  
Pelt J., Schild R., Refsdal S., Stabell R., 1998, A&A 336, 829  
Refsdal S., Stabell R., 1991, A&A 250, 62 (RS1)  
Refsdal S., Stabell R., 1993, A&A 278, L5 (RS2)  
Refsdal S., Stabell R., 1997, A&A 325, 877  
Schild R., Smith R. C., 1991, AJ 101, 813  
Schild, R., 1996, ApJ 464, 125  
Schmidt R., Wambsganss J., 1998, A&A 335, 379  
Schneider P., Weiss A., 1987, A&A 171,49  
Vanderriest C., Schneider J., Herpe G., et al., 1989, A&A 215, 1  
Wambsganss, J. and Kundić, T., 1995, ApJ 450, 19  
Wyithe J.S.B., Webster R.L., Turner E., 1999, submitted to MNRAS